

cells make contact with an APC, arrest, and depolarize, forming a small cluster as cells accumulate; subsequently, the clustered cells enlarge and begin to swarm before they undergo cell division.

This report introduces two-photon microscopy as a powerful tool for immunological studies that permits noninjurious imaging of individual living immune cells deep within highly scattering tissues. In addition to providing 3D resolution of cell morphology and permitting tracking of cell motility with a time resolution of a few seconds, successive cycles of cell division can be followed by means of the serial dilution of fluorescent label. The techniques described here may be applicable to other tissues (such as the thymus, spleen, and sites of inflammation), to other cell types (including APCs), to intravital imaging within intact organs, and to the use of fluorescent probes that signal cell function (such as Ca²⁺ signaling and gene expression).

References and Notes

1. A. J. Young, *Semin. Immunol.* **11**, 73 (1999).
2. S. K. Bromley *et al.*, *Annu. Rev. Immunol.* **19**, 375 (2001).
3. M. L. Dustin, A. R. de Fougerolles, *Curr. Opin. Immunol.* **13**, 286 (2001).
4. M. K. Jenkins *et al.*, *Annu. Rev. Immunol.* **19**, 23 (2001).
5. Q. T. Nguyen, N. Callamaras, C. Hsieh, I. Parker, *Cell Calcium* **30**, 383 (2001).
6. W. Denk, K. Svoboda, *Neuron* **18**, 351 (1997).
7. BALB/c CD3⁺ T lymphocytes from peripheral lymph nodes and naïve BALB/c CD19⁺ B lymphocytes from the spleen were enriched by negative selection to >98% purity by magnetic depletion using anti-MHC II MicroBeads (MHC, major histocompatibility complex) or anti-CD43 MicroBeads, respectively (Miltenyi Biotec, Auburn, CA). For purification of DO11.10 CD3⁺ T cells, a combination of anti-MHC II MicroBeads and DX5 anti-natural killer cell MicroBeads was used as above. Cells were stained for 30 min at 37°C with 2 μM CFSE or CMTMR, destined, and washed with serum-free medium. Cells were resuspended in phosphate-buffered saline and adoptively transferred by tail vein injection into recipient BALB/c mice 4 to 6 weeks of age. For cell-tracking experiments, 10 million to 12 million purified CFSE-labeled T or B lymphocytes were adoptively transferred. Lymph nodes were harvested from the recipient mice 18 to 20 hours after adoptive transfer and were mounted in the imaging chamber. To observe the reticular fiber network, we counterstained lymph nodes in 2 μM CMTMR in serum-free medium for 45 min at room temperature and then destined and washed them. The labeling was stable for at least 1 hour under our imaging conditions.
8. Two-photon imaging was done with a custom-built, video-rate multiphoton microscope (5), using an upright Olympus BX50 microscope fitted with a ×20 water-immersion objective (numerical aperture = 0.95), a Spectra-Physics Tsunami femtosecond laser, and a resonant-mirror scan head. Image acquisition, a z-axis stepper, shutters, and an emission filter wheel were under software control (MetaMorph, Universal Imaging, Downingtown, PA). Lymph nodes were cemented to the base of the imaging chamber with a thin film of veterinary-grade superglue and were continuously superfused with warm (35° to 37°C) RPMI 1640 medium bubbled with 95% O₂ and 5% CO₂. For imaging lymphocyte motility, 5D image stacks (x, y, z, time, and emission wavelength) were acquired as follows. Each xy plane spanned 200 μm by 200 μm at a resolution of 2 pixels μm⁻¹ and was formed by averaging nine video frames. Alternate images at each plane were acquired at emission

- wavelengths of 510 to 550 nm (for CFSE-labeled cells) and 600 to 700 nm (for CMTMR-labeled cells), selected by a computer-controlled filter wheel. For each time point (10-s intervals), a stack of 17 two-color planes was acquired at axial (z) spacings of 3 μm, with a computer-controlled focus motor. After recording, image stacks were processed to yield maximum-intensity projections representing "top" (xy) or "side" (xz) views through the scanned volume of the lymph node. For single-label experiments with CFSE, excitation at 780 nm provided an optimal signal. For dual-label experiments, the laser was tuned to 820 nm so as to equally excite both fluorophors.
9. K. M. Murphy, A. B. Heimberger, D. Y. Loh, *Science* **250**, 1720 (1990).
10. For antigenic challenge, recipient BALB/c mice were primed by subcutaneous injections with 150 μl of a 1.3% alum emulsion containing 3 μg of ovalbumin and 600 to 800 ng of murine tumor necrosis factor-α (Stemcell Technologies, Vancouver, BC). About 50 μl were injected into three sites on each mouse that were chosen to enhance the delivery of antigen to draining cervical and inguinal lymph nodes. DO11.10 T cells were purified and labeled with CFSE, and 10 million to 12 million CD3⁺ T cells were adoptively transferred either into antigen-primed mice 24 hours after antigenic challenge or into unprimed recipient mice. At 1 and 5 days after adoptive transfer, the nodes of antigen-primed animals and of unprimed

- control animals were placed side by side in the recording chamber for sequential imaging.
11. M. Gunzer *et al.*, *Immunity* **13**, 323 (2000).
12. P. Friedl, K. S. Zanker, E. B. Brocker, *Microsc. Res. Tech.* **43**, 369 (1998).
13. P. Friedl, P. B. Noble, E. D. Shields, K. S. Zanker, *Immunology* **82**, 617 (1994).
14. P. A. Negulescu, T. B. Krasieva, A. Khan, H. H. Kerschbaum, M. D. Cahalan, *Immunity* **4**, 421 (1996).
15. C. Elenstrom-Magnusson, W. Chen, B. Clinchy, B. Obrink, E. Severison, *Int. Immunol.* **7**, 567 (1995).
16. J. E. Gretz, C. C. Norbury, A. O. Anderson, A. E. I. Proudfoot, S. Shaw, *J. Exp. Med.* **192**, 1425 (2000).
17. T. E. DeCoursey, K. G. Chandy, S. Gupta, M. D. Cahalan, *J. Gen. Physiol.* **89**, 405 (1987).
18. We thank A. Hejazi for help with cell tracking, L. Forest for care and breeding of the DO11.10 mouse strain, and G. Gutman and G. Chandy for helpful suggestions and comments on the manuscript. Supported by NIH grants GM-48071 (I.P.) and GM-41514 (M.D.C.).

Supporting Online Material

www.sciencemag.org/cgi/content/full/1070051/DC1
 Movies S1 to S6

22 January 2002; accepted 12 April 2002
 Published online 16 May 2002;
 10.1126/science.1070051

Include this information when citing this paper.

Dynamic Imaging of T Cell–Dendritic Cell Interactions in Lymph Nodes

Sabine Stoll,¹ Jérôme Delon,¹ Tilmann M. Brotz,^{2*} Ronald N. Germain^{1†}

T cell immune responses begin within organized lymphoid tissues. The pace, topology, and outcomes of the cellular interactions that underlie these responses have, so far, been inferred from static imaging of sectioned tissue or from studies of cultured cells. Here we report dynamic visualization of antigen-specific T cells interacting with dendritic cells within intact explanted lymph nodes. We observed immunological synapse formation and prolonged interactions between these two cell types, followed by the activation, dissociation, and rapid migration of T cells away from the antigenic stimulus. This high-resolution spatiotemporal analysis provides insight into the nature of cell interactions critical to early immune responses within lymphoid structures.

Naïve T lymphocytes circulate through the blood and lymph between sojourns within secondary lymphoid tissues (1), where they scan peptide–major histocompatibility complex molecule (p-MHC) ligands displayed on the plasma membranes of dendritic cells (DCs) (2). If accompanied by appropriate co-signals (3), ligand recognition induces T cell clonal expansion together with differentiation that promotes migration either to B

cell areas to assist in antibody production (4, 5) or out of the lymphoid tissue to sites of inflammation (1).

Our current view of T cell localization within lymphoid organs and of lymphocyte interaction with antigen-bearing cells derives mainly from static immunohistochemical or fluorescence imaging of cells in tissue sections (6) or from static and video microscopic analysis of T cell–antigen-presenting cell (APC) interaction in in vitro models (7–11). What is missing is a dynamic, high-resolution view of these events in the more complex, physiological environment of organized lymphoid tissue. To provide this missing information, we have developed a method for extended four-dimensional confocal imaging of T cells and DCs within intact mouse lymph nodes (LNs). In a variation of the technique established by Ingulli *et al.* (12), we labeled

¹Lymphocyte Biology Section, Laboratory of Immunology, National Institute of Allergy and Infectious Diseases, National Institutes of Health, ²Experimental Immunology Branch, National Cancer Institute, National Institutes of Health, Bethesda, MD 20892, USA.

*Present address: 270 Littlefield Avenue, South San Francisco, CA 94080, USA.

†To whom correspondence should be addressed. E-mail: rgermain@nih.gov

REPORTS

naïve T cells from T cell receptor (TCR) transgenic mice and bone marrow–derived DCs of the correct MHC type with distinct fluorescent dyes (13). After labeling with or without antigen exposure, the DCs were injected subcutaneously, which led to their migration to the draining LN [see note S1 (13) for a detailed discussion of DC phenotype and accumulation in the LN]. The labeled T cells were then introduced intravenously after a suitable interval (typically 6 hours in this study). Both DCs and T cells were found in the expected regions of the LN in tissue sections [fig. S1 (13)]. Later, at various time points, the LN was removed and imaged. In this way, different periods of the immune response could be visualized, with each continuous imaging data collection set spanning up to 15 hours. [See note S2 (13) for a discussion of tissue state and phototoxicity under these imaging conditions.]

If T cells were transferred into animals that received antigen-free DCs in one footpad and antigen-bearing DCs in the other, a substantially greater number of T cells accumulated 18 hours later in the LN with the antigen-bearing APC [with antigen/without antigen = 3.35 ± 1

($n = 3$); Fig. 1, A and B]. A few T cells established close contacts with the foreign antigen-free DCs (Fig. 1A, squares). These foreign antigen-independent associations occasionally lasted several hours, but the T cells did not become activated [fig. S2 (13)].

In the draining LN with antigen-bearing DCs, the more abundant antigen-specific T cells were primarily found in one-to-one association with the APC (Fig. 1B, circles). If both antigen-bearing and antigen-free DCs were in the same LN, T cells showed a preferential association with antigen-pulsed DCs [$65 \pm 8\%$ ($n = 3$); Fig. 1D, circles] compared with the antigen-free DCs (Fig. 1C, squares). Cell couples involving antigen-bearing DCs were very long-lived and showed continuous tight association throughout a 15-hour observation period [Fig. 1E; movies S1 to S3 (13)]. At the end of this time, an average of $68 \pm 2\%$ ($n = 3$) of the transferred T cells in the LN with antigen-bearing DCs had become CD69^{high} [fig. S2 (13)], indicating they had been activated. The difference in T cell numbers in LNs with antigen-free versus antigen-bearing DCs appears to reflect the longer lived associations

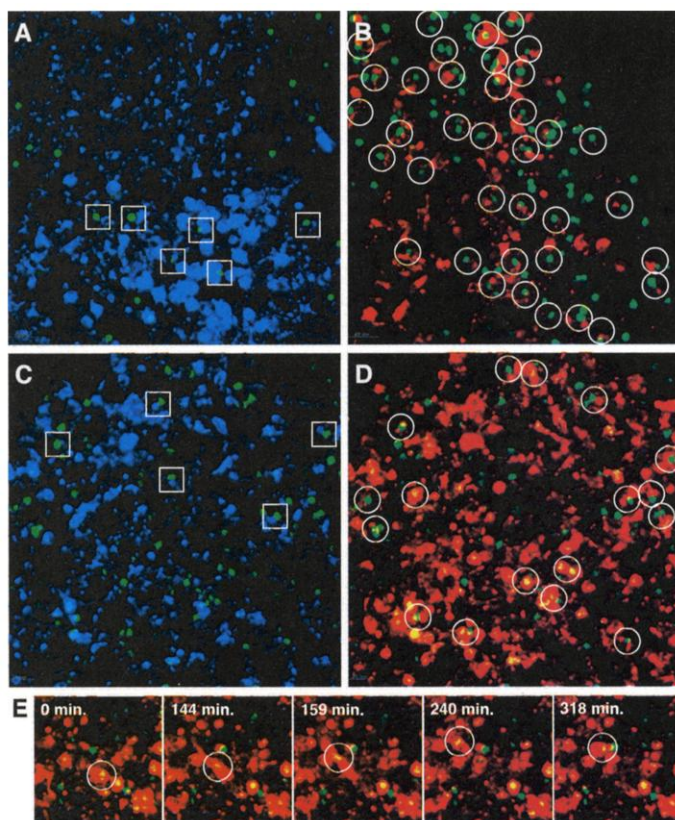
of T cells with the latter APC, leading to accumulation of the lymphocytes instead of their reentry into the circulation.

T cells exposed to antigen-bearing DCs behaved differently when the observation window was shifted to >37 hours after T cell transfer. Now, many of the lymphocytes moved rapidly through the tissue at 5 to $7 \mu\text{m}/\text{min}$ instead of remaining associated with a DC [movies S4 to S6 (13)]. The paths followed by migrating T cells over a 3-hour period were traced (Fig. 2), revealing the changing direction of many of the cells over time (Fig. 2, A and B). Together with the preceding data (Fig. 1), these results indicate that T cells arrested their movement early after exposure to antigen-bearing DCs, as observed previously in vitro (14); they also formed long-lived associations with a single APC. After 36 to 48 hours, these cells showed evidence of activation, began to dissociate from the DCs that provided the original antigenic stimulus, and migrated rapidly within the LN [see notes S2 and S3 (13) for discussions of why chemokine desensitization, altered oxygenation, and laser phototoxicity are unlikely to account for these observations]. This timing is in general agreement with earlier studies showing that, in the presence of antigen, T cells are sequestered from the circulation for 2 to 4 days before they exit into the efferent lymph (1, 15).

We also observed T cells undergoing division after interaction with an antigen-bearing DCs [Fig. 3; movie S7 (13)]. The process took 5 hours and the daughter cells eventually migrated away, providing evidence that cell movement is associated with the activation process. We first observed such cell divisions beginning at the 37-hour time point, which agrees with evidence that proliferation of naïve T cells exposed to antigen in vivo occurs after a lag period of 1.5 to 2 days (16).

Molecular partitioning occurs at the zone of membrane contact between T cells and antigen-bearing APC in vitro (7, 9, 11). One characteristic aspect of this protein redistribution is the moesin-dependent exclusion of CD43 from the central and peripheral supramolecular activations cluster (c- and pSMAC) areas of the immunological synapse (17). Therefore, we used this imaging scheme to examine whether this pattern of CD43 localization was also found with T cells and APC interacting within LNs. Mobilized bone marrow cells from TCR transgenic donors were infected with retrovirus encoding a CD43–green fluorescent protein (GFP) chimeric molecule (13), and the transduced bone marrow cells were then used to generate radiation chimeras. This produces mature naïve CD43–GFP–expressing T cells that show high rates of LN homing (18). After transfer into mice of CD43–GFP transduced T cells stained with a red cytoplasmic dye, synapses were visualized as regions of membrane contact between red T cells and blue antigen-bearing DCs from which green CD43–GFP molecules were

Fig. 1. Effect of antigen on T cell–DC interactions in situ. (A and B) DiD-stained (blue) or Dil-labeled (red) antigen-bearing DCs were separately injected subcutaneously in the opposite hind footpads of a mouse. Six hours later, 5-carboxyfluorescein diacetate succinyl ester (CFSE)-loaded (green) 5C.C7 CD4⁺ TCR transgenic T cells were injected intravenously. Popliteal LNs were imaged 18 hours later. More T lymphocytes are retained in the LN containing antigen-pulsed DCs. T cell–DC conjugates are marked with white squares [(A), unpulsed] and white circles [(B), pulsed]. (C and D) Dil-labeled antigen-bearing and DiD-stained antigen-free DCs were coinjected subcutaneously into a single hind footpad. Six hours later, CFSE-loaded T lymphocytes were injected intravenously. Popliteal LNs were imaged 20 hours later. T cells preferentially establish stable contact with antigen-bearing rather than antigen-free DCs when both APC are present in the same lymphoid organ. T cell–DC conjugates are marked with white squares [(C), unpulsed] and white circles [(D), pulsed]. Green T cells superimposed over an associated red DC appear yellow. (E) Close-up, sequential views of a field in which several T lymphocytes have formed conjugates with antigen-bearing DCs. Over the 5.3 hours illustrated, each T cell remains in association with the same DC, although changes in shape of the cells and even migration of one DC with an attached T cell can be observed (circles). The time of the first image is arbitrarily set to 0 min.



excluded (Fig. 4). A similar exclusion of CD43-GFP from regions of membrane contact with antigen-free DCs was also occasionally observed (19) [see note S4 (13) for further discussion of CD43 distribution on T cells in LNs]. These findings extend previous tissue section studies that suggest formation of prototypic immunological synapses in vivo (20).

This report describes direct dynamic visualization of T cell–DC interactions within non-sectioned lymphoid tissue at high spatial and temporal resolution. Although an isolated LN lacks blood and lymph flow [which may alter oxygen tension (21) and chemokine gradients (1, 4)] and does not possess neuronal connections, the method described here provides a stable platform for imaging over prolonged periods that is difficult to duplicate with available intravital approaches [see note S5 (13) for additional discussion of this issue]. With this technique, we find that CD4⁺ T cells form long-lived (>15 hours) associations with an individual antigen-bearing DC before activation and induced migration. When offered a choice of antigen-bearing and antigen-free DCs, the T cells preferentially associate with the APC-bearing stimulatory ligand, as previously observed in vitro (22). Cell division was visualized, as were immunological synapses defined by the exclusion of CD43 (17).

The long-lived associations observed here with naïve T cells and antigen-bearing DCs fit an evolving model of lymphocyte activation that entails reciprocal communication between these two cell types (23–26) and support the view that a naïve T cell engages a single DC for the time necessary to complete this back-and-forth molecular conversation. This, in turn, ensures that the fate of the stimulated T cell is dictated by the differentiation state of the DC whose antigen display initiated its activation (3, 24). These imaging data agree with older in vitro data (27) but contrast with recent experiments using collagen gel matrices in vitro that showed multiple transient (<15 min) sequential lymphocyte-APC contacts, eventually leading to lymphocyte activation (10).

The confocal imaging method used here allows visualization only to 80 μm, which is inadequate for examining the more centrally located T cell zones, where DCs concentrate and T lymphocytes enter via high endothelial venules (1). For this reason, we have so far been unable to determine whether T cells show the short-lived interactions reported in the collagen gel matrix model (10) before they establish a prolonged association with a particular DC or whether they prelocalize CD43 to the trailing uropod (28) [see note S4 (13) for additional discussion]. Multiphoton instruments permit imaging deeper within tissues and with less potential photodamage (29). Applying this technology to the general methods described here for visualization of

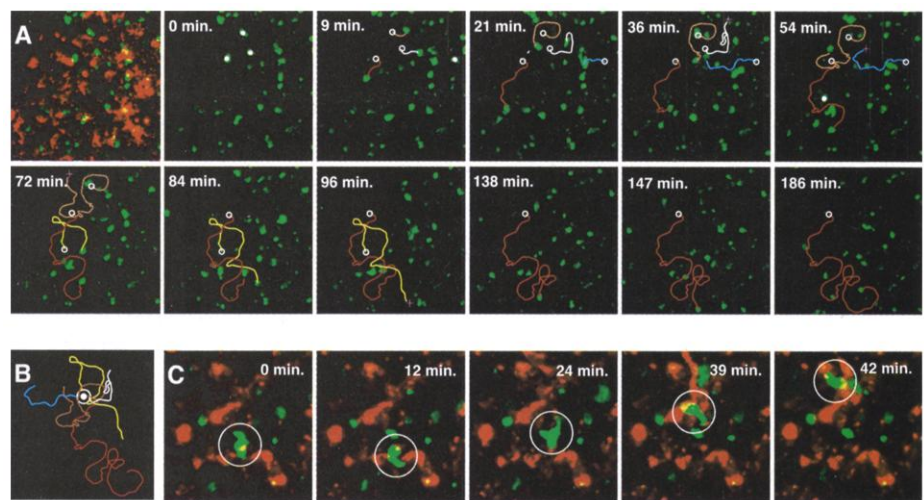


Fig. 2. Analysis of T cell migration in a LN. Dil-labeled antigen-bearing DCs were injected subcutaneously in the hind footpad. Six hours later, CFSE-loaded T lymphocytes were injected intravenously. Popliteal LNs were imaged 37 hours later. (A) Movement of individual T cells. In the first image, both T cells and DCs are shown for orientation. In the images that follow, only the T cells are shown. The time of collection of the first image is arbitrarily set to 0 min. A white dot indicates the first appearance of a T cell in the field. The paths followed by individual T cells are plotted as colored lines (73). When a particular cell disappears from the field, its last position is indicated by a white cross, and its path is omitted in succeeding images. (B) Superimposition of the paths of the five T cells tracked in (A). The initial position of each cell is arbitrarily placed at the same location. The different directions taken by T cells in the same region of the LN and the changing orientation of T cells as they move are clearly shown. (C) Higher magnification sequence illustrating rapid migration of a single T cell (circles). The time of collection of the first image is arbitrarily set to 0 min.

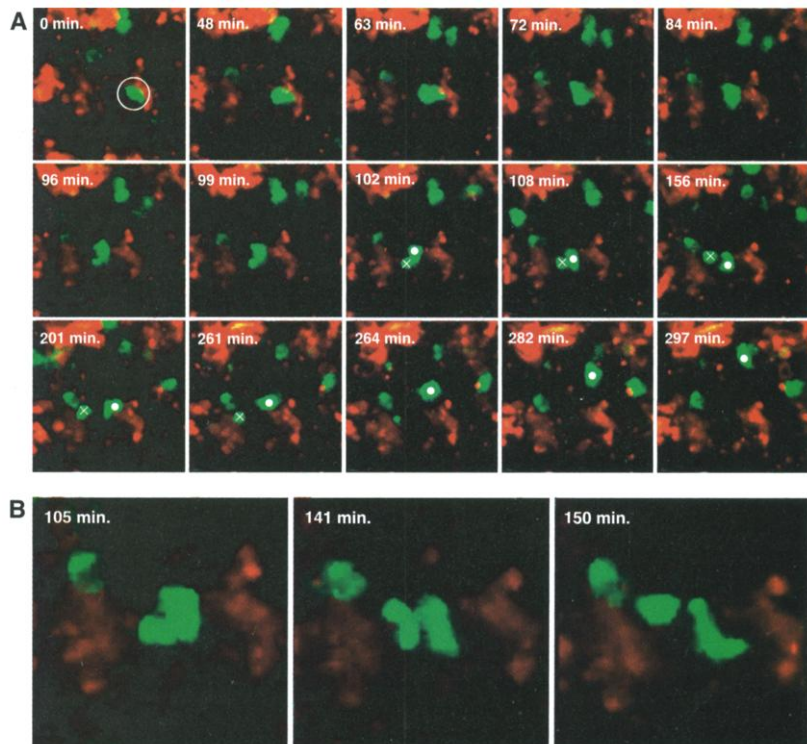


Fig. 3. Visualization of T cell division in situ. Dil-labeled antigen-bearing DCs were injected subcutaneously in the hind footpad. Six hours later, CFSE-loaded T lymphocytes were injected intravenously. Popliteal LNs were imaged 37 hours later. Cell division beginning 10 hours later is shown. The time of collection of the first image is arbitrarily set to 0 min. (A) The two daughter cells are highlighted with a dot and a cross in the first frame in which they are distinctly visible (102 min). After the two daughter cells are formed, one rapidly dissociates from the stimulatory DC (156 min) and then disappears deeper into the LN (261 to 282 min), whereas the other moves away from the DC more slowly (264 to 297 min). (B) Higher magnification views of the dividing cell. Times marked are on the same scale as those in (A).

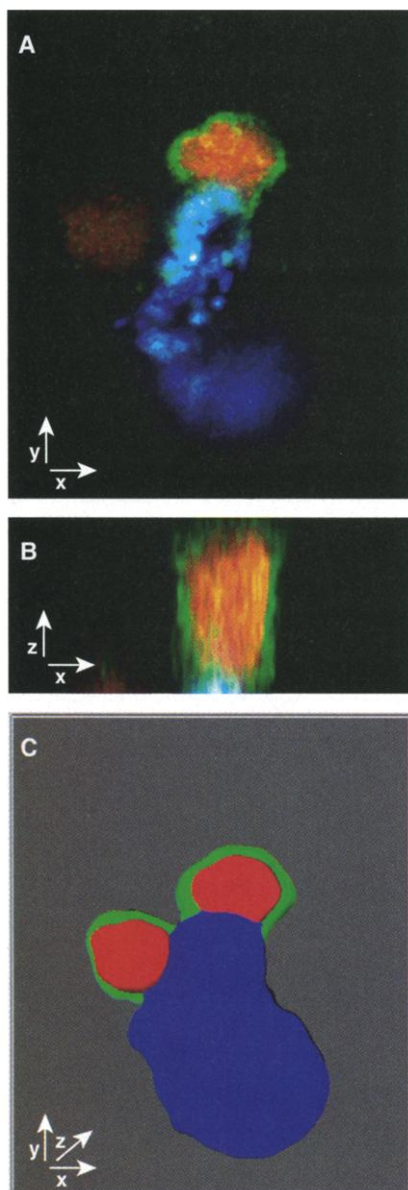


Fig. 4. Observation of immunological synapse formation inside a LN. SNARF-labeled (red) naïve CD43-GFP⁺ T cells (13) were injected intravenously into mice given DiD-labeled antigen-pulsed DCs 12 hours before. Popliteal LNs were imaged 23 hours later by acquiring a series of z sections throughout the contact region. **(A)** One section through the equatorial plane of the synapse shows exclusion of the green signal coming from the CD43-GFP. **(B)** The en face view shows that this pattern of exclusion is quite broad with a peripheral ring of CD43 surrounding a central region labeled with the cytoplasmic red dye. **(C)** A three-dimensional representation of the merged sections shows that the two T cells bound to this DC both exclude CD43 from the zone of membrane contact (synapse).

hematopoietic cell interactions in architecturally intact lymphoid tissue will open an even more complete window on the events involved in antigen-specific immune reactions.

References and Notes

1. E. C. Butcher, M. Williams, K. Youngman, L. Rott, M. Briskin, *Adv. Immunol.* **72**, 209 (1999).
2. I. Mellman, R. M. Steinman, *Cell* **106**, 255 (2001).
3. C. Reis e Sousa, *Immunity* **14**, 495 (2001).
4. J. G. Cyster, *Science* **286**, 2098 (1999).
5. M. K. Jenkins et al., *Annu. Rev. Immunol.* **19**, 23 (2001).
6. P. Garside et al., *Science* **281**, 96 (1998).
7. C. R. Monks, B. A. Freiberg, H. Kupfer, N. Sciaky, A. Kupfer, *Nature* **395**, 82 (1998).
8. J. Delon, N. Bercovici, G. Raposo, R. Liblau, A. Trautmann, *J. Exp. Med.* **188**, 1473 (1998).
9. A. Grakoui et al., *Science* **285**, 221 (1999).
10. M. Gunzer et al., *Immunity* **13**, 323 (2000).
11. M. F. Krummel, M. D. Sjaastad, C. Wülfing, M. M. Davis, *Science* **289**, 1349 (2000).
12. E. Ingulli, A. Mondino, A. Khoruts, M. K. Jenkins, *J. Exp. Med.* **185**, 2133 (1997).
13. Supporting online material is available on Science Online at www.sciencemag.org/cgi/content/full/296/5574/1873/DC1.
14. M. L. Dustin, S. K. Bromley, Z. Kan, D. A. Peterson, E. R. Unanue, *Proc. Natl. Acad. Sci. U.S.A.* **94**, 3909 (1997).
15. J. Sprent, J. F. Miller, G. F. Mitchell, *Cell. Immunol.* **2**, 171 (1971).
16. C. Tanchot, D. L. Barber, L. Chiodetti, R. H. Schwartz, *J. Immunol.* **167**, 2030 (2001).
17. J. Delon, K. Kaibuchi, R. N. Germain, *Immunity* **15**, 691 (2001).
18. G. A. Hollander, B. D. Luskey, D. A. Williams, S. J. Burakoff, *J. Immunol.* **149**, 438 (1992).
19. S. Stoll, unpublished observations.
20. P. Reichert, R. L. Reinhardt, E. Ingulli, M. K. Jenkins, *J. Immunol.* **166**, 4278 (2001).
21. C. C. Caldwell et al., *J. Immunol.* **167**, 6140 (2001).
22. S. Valitutti, S. Muller, M. Dessing, A. Lanzavecchia, *Eur. J. Immunol.* **26**, 2012 (1996).
23. J. Banchereau, R. M. Steinman, *Nature* **392**, 245 (1998).
24. C. Reis e Sousa, A. Sher, P. Kaye, *Curr. Opin. Immunol.* **11**, 392 (1999).
25. J. Delon, R. N. Germain, *Curr. Biol.* **10**, R923 (2000).
26. R. N. Germain, *Science* **293**, 240 (2001).
27. P. E. Lipsky, A. S. Rosenthal, *J. Exp. Med.* **141**, 138 (1975).
28. J. M. Serrador et al., *Blood* **91**, 4632 (1998).
29. P. T. So, C. Y. Dong, B. R. Masters, K. M. Berland, *Annu. Rev. Biomed. Eng.* **2**, 399 (2000).
30. We thank O. Schwartz (National Institute of Allergy and Infectious Diseases confocal facility) for help with the acquisition of images. Supported by post-doctoral fellowships from the Deutsche Forschungsgemeinschaft (S.S.) and the Human Frontier Science Program (J.D.).

20 February 2002; accepted 25 April 2002

Dynamics of Thymocyte–Stromal Cell Interactions Visualized by Two-Photon Microscopy

Philippe Bousso,¹ Nirav R. Bhakta,^{2*} Richard S. Lewis,² Ellen Robey^{1†}

Thymocytes are selected to mature according to their ability to interact with self major histocompatibility complex (MHC)–peptide complexes displayed on the thymic stroma. Using two-photon microscopy, we performed real-time analysis of the cellular contacts made by developing thymocytes undergoing positive selection in a three-dimensional thymic organ culture. A large fraction of thymocytes within these cultures were highly motile. MHC recognition was found to increase the duration of thymocyte–stromal cell interactions and occurred as both long-lived cellular associations displaying stable cell–cell contacts and as shorter, highly dynamic contacts. Our results identify the diversity and dynamics of thymocyte interactions during positive selection.

Tissue microenvironments are likely to have a profound impact on lymphocyte behavior, yet most studies of lymphocytes have relied on monolayer cultures or fixed-tissue preparations that fail to recapitulate the complexity and the dynamics of cellular environments. With respect to T cell development, fundamental questions remain about how thymo-

cytes behave within the three-dimensional stromal cell network required for their differentiation. Generation of an efficient repertoire of mature $\alpha\beta$ T lymphocytes by positive selection is governed by interactions between the T cell antigen receptor (TCR) of immature CD4⁺CD8⁺ double-positive (DP) thymocytes and the array of self MHC–peptide complexes displayed on the surface of thymic stromal cells (1–3). The patterns of thymocyte motility during this process, the dynamics and the topology of thymocyte–stromal cell interactions, and the influence of MHC recognition on these cellular contacts have yet to be characterized.

The advent of two-photon laser scanning microscopy (TPLSM) offers a powerful

¹Department of Molecular and Cell Biology, University of California, Berkeley, CA 94720, USA. ²Department of Molecular and Cellular Physiology, Stanford University School of Medicine, Stanford, CA 94305, USA.

*This author made independent, essential contributions to this work.

†To whom correspondence should be addressed. E-mail: erobey@uclink4.berkeley.edu